arXiv:1703.00832v2 [cs.CV] 7 Mar 2017

Face Image Reconstruction from Deep Templates

Guangcan Mai, *Student Member, IEEE,* Kai Cao, Pong C. Yuen, *Senior Member, IEEE,* and Anil K. Jain, *Life Fellow, IEEE*

Abstract—State-of-the-art face recognition systems are based on deep (convolutional) neural networks. Therefore, it is imperative to determine to what extent face templates derived from deep networks can be inverted to obtain the original face image. In this paper, we discuss the vulnerabilities of a face recognition system based on deep templates, extracted by deep networks under image reconstruction attack. We propose a de-convolutional neural network (D-CNN) to reconstruct images of faces from their deep templates. In our experiments, we did not assume any knowledge about the target subject nor the deep network. To train the D-CNN reconstruction models, we augmented existing face datasets with a large collection of images synthesized using a face generator. The proposed reconstruction method was evaluated using type-I (comparing the reconstructed images against the original face images used to generate the deep template) and type-II (comparing the reconstructed images against a different face image of the same subject) attacks. We conducted a three-trial attack for each target face image using three face images reconstructed from three different D-CNNs. Each D-CNN was trained on a different dataset (VGG-Face, CASIA-Webface, or Multi-PIE). The type-I attack achieved a true accept rate (TAR) of 85.48% at a false accept rate (FAR) of 0.1% on the LFW dataset. The corresponding TAR for the type-II attack is 14.71%. Our experimental results demonstrate the need to secure deep templates in face recognition systems.

Index Terms—Face recognition, template security, deep networks, deep templates, image reconstruction, de-convolutional neural network.

1 Introduction

Face recognition systems are being increasingly used in applications ranging from social networks (image tagging) to security systems (e.g., banking[1] and border control[2]). In critical applications, face recognition needs to meet stringent performance requirements, including low error rates and strong system security. In particular, the system must be resistant to spoofing and template attacks. Therefore, it is critical to evaluate the vulnerabilities of a face recognition system to these two types of attacks, and devise countermeasures, before it is deployed. To this end, several attack mechanisms (such as hill climbing [1], [2], [3], [4], spoofing [5], [6], [7], [8], and image reconstruction (template invertibility) [9]) have been proposed to determine the vulnerabilities of face recognition systems.

In this paper, we focus on the vulnerability of a face recognition system to template invertibility or image reconstruction attack. In an image reconstruction attack (Fig. 1), we want to determine if face images can be reconstructed from the face templates of target subjects. The goal is then to determine whether a face recognition system can be successfully attacked by fake faces, such as a 3D mask created from the reconstructed images (a spoofing attack), or by directly presenting the reconstructed images to the feature extractor module in Fig. 1. Fig. 2 shows examples of face images reconstructed from their deep templates by the proposed method. Some of these reconstructions are successful in that they match well with the original images (Fig. 2a), while others are not successful (Fig. 2b). Image reconstruction attacks assume that templates of target subjects and the corresponding *black-box* template extractor can be accessed. These are reasonable assumptions because: (a) templates of target users can be exposed in hacked databases[3], and (b) the corresponding *black-box* template extractor can potentially be obtained by purchasing the face recognition SDK.

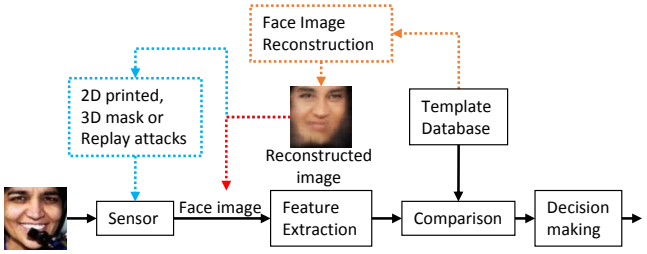

Fig. 1. Face recognition system vulnerability to image reconstruction attacks. Face image of a target subject is reconstructed from a template to gain system access by either (a) creating a fake face (for example, a 2D printed image or 3D mask) (blue box) or (b) inserting a reconstructed face into the feature extractor (red box).

Face templates are typically compact binary or real-valued feature representations[4] that are extracted from face images to increase storage efficiency and the efficiency and

- *Guangcan Mai and Pong C. Yuen are with the Department of Computer Science, Hong Kong Baptist University, Kowloon, Hong Kong. E-mail: {csgcmai,pcyuen}@comp.hkbu.edu.hk*
- *Kai Cao and Anil K. Jain are with the Department of Computer Science and Engineering, Michigan State University, MI, 48824. E-mail: {kaicao,jain}@cse.msu.edu*

1. http://www.zdnet.com/article/china-developing-atm-with-face-recognition/
2. http://www.latimes.com/local/california/la-me-1213-border-biometrics-20151213-story.html
3. http://www.forbes.com/sites/leemathews/2016/12/16/what-to-do-if-you-think-your-yahoo-account-was-hacked/
4. As face templates refer to face representations stored in a face recognition system, these terms are used interchangeably in this paper.

TABLE 1
Comparison of major face image reconstruction algorithms

Algorithm	Template features	Evaluation	Remarks
MDS [10]	PCA, BIC, COTS	Type-I attack[a]: TAR of 72% using *BIC*[b] and 73% using *COTS*[c] at an FAR of 1.0% on FERET	Linear model with limited capacity
RBF regression [9]	LQP [11]	Type-II attack[d]: 20% rank-1 identification error rate on FERET; EER = 29% on LFW	RBF model may have limited generative capacity
Proposed	FaceNet [12]	[e]Type-I attack: TAR[f] of 85.48% (LFW) and 26.58% (FRGC v2.0) at an FAR of 0.1%. Type-II attack: TAR of 14.71% (LFW) and 16.60% (FRGC v2.0) at an FAR of 0.1%	Requires a large number of images for network training

[a] Type-I attack refers to matching the reconstructed image against the face image from which the template was extracted.
[b] *BIC* refers to Bayesian intra/inter-person classifier [13].
[c] *COTS* refers to commercial off-the-shelf system. A local-feature-based COTS was used in [10].
[d] Type-II attack refers to matching the reconstructed image against a face image of the same subject that was not used for template creation.
[e] Based on a fusion of decisions of attacking each target face using three face images reconstructed with three different D-CNNs.
[f] TAR for LFW and FRGC v2.0 cannot be directly compared because their similarity thresholds differ.

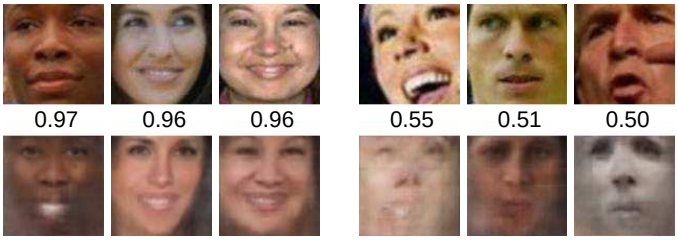

(a) Successful match (b) Unsuccessful match

Fig. 2. Example face images reconstructed from their templates using the proposed method (CASIA-Gen). The top row shows the original images (from LFW) and the bottom row shows the corresponding reconstructions. The numerical value shown between the two images is the cosine similarity between the original face image and its reconstructed image. The verification thresholds are 0.78 and 0.66 at FAR = 0.1 and 1.0%, respectively.

accuracy of similarity computation. Over the past couple of decades, a large number of approaches have been proposed for creating face representations. These representations can be broadly categorized into either shallow [14], [15], [16], [17], [18], [19] or deep (convolutional neural network or CNN) representations [12], [20], [21], [22], [23], according to the depth of their representational model[5]. Deep CNN representations are preferred because of their superior performances in face evaluation benchmarks (such as Labeled Faces in the Wild (LFW) [24], YouTube Faces [12], [25], and NIST IJB-A [26]). Therefore, it is imperative to investigate the invertibilities of deep templates to determine their vulnerability to image reconstruction attacks. However, to the best of our knowledges, no such work has yet been reported.

In our study of image reconstruction attacks, we made no assumptions about subjects in the target face recognition system. Therefore, only public domain face images were used to train the image reconstruction model. The available algorithms for face image reconstruction from templates [9] [10][6] are summarized in Table 1. The generalizability of these image reconstruction attacks is not known, as all of the training and testing images used in their evaluations were subsets of the same face dataset.

Reconstructing face images from deep templates requires inverting the complex mapping used in the deep template extraction model [27]. Furthermore, deep templates may not contain sufficient details for reconstructing face images because they are high-level abstractions of face image data. Current image reconstruction methods [9], [10] are based on shallow models, which have limited capacities for modeling complex mapping between deep templates and face images (Section 2.1). Consequently, current methods are not able to reconstruct face images from deep templates.

To determine to what extent face templates derived from deep networks can be inverted to obtain the original face image, a reconstruction model with sufficient capacity to model complex mapping between deep templates and face images is needed. Different from shallow models such as dictionary learning [28], [29] (either linear or non-linear kernels) that provides limited capacity, we propose a deconvolutional neural network (D-CNN)[7] [30], [31] based method. In contrast to a CNN, which hierarchically abstracts face images to generate templates, a D-CNN inverts the templates to reconstruct the face images layer by layer. By stacking multiple non-linear network layers, a D-CNN is able to model complex mapping between deep templates and face images. As no prior knowledge regarding a target subject is assumed, the learned D-CNN is expected to be highly generalizable. To train the D-CNN, a large number of face images are required. Instead of following the time-consuming and expensive process of collecting a sufficiently large face dataset [32], [33], we trained a face image generator [34] to augment available public domain face datasets.

In summary, this study makes the following main contributions.

- The invertibility of face templates generated by deep networks was investigated. No prior knowledge about target subjects in the target face recognition system was required. To the best of our knowledge, this is the first study to address the security aspects of deep templates.

5. Some researchers [22] refer to shallow representations as those that are not extracted using deep networks.

6. The MDS method was initially proposed for reconstructing templates by matching scores between the target subject and attacking queries. However, it can also be used for image reconstruction attacks [9].

7. Some researches refer to D-CNNs as CNNs. However, given that its purpose is the inverse of a CNN, we prefer the term D-CNN.

- A D-CNN based method was developed to reconstruct face images from deep templates. The proposed D-CNN has sufficient model capacity so that it can learn to reconstruct face images from deep templates.
- A face image generator was used to augment publicly available face datasets for training D-CNNs. Three D-CNNs, called VGG-Gen, CASIA-Gen, and Multi-PIE-Gen, were trained for image reconstruction. Based on a decision-level fusion of three face images reconstructed from three separately trained D-CNNs, a type-I attack achieved a true accept rate (TAR) of 85.48% (26.58%) on LFW (FRGC v2.0), with a false accept rate (FAR) of 0.1%. The TAR of the corresponding type-II attack was 14.71% (16.60%) on LFW (FRGC v2.0).

The rest of this paper is organized as follows. Section 2 briefly reviews several methods for reconstructing face images from shallow templates and several D-CNN based approaches for face image generation. The proposed D-CNN-based approach for inverting deep face templates is described in Section 3. In Section 4, we present a security analysis of deep templates, in terms of the accuracies of type-I and type-II image reconstruction attacks. Finally, we make concluding remarks and describe our plans for future work in Section 5.

2 Related Work

In this section, we describe the limitations of current methods in reconstructing face images from deep templates, and introduce D-CNNs for generating synthetic face images.

2.1 Reconstructing Face Images from Deep Templates

Face image reconstruction requires the determination of the inverse of deep models [12], [20], [21], [22], [23], which extract deep templates from face images. Most deep models are complex. They are typically implemented by designing a network with sufficiently large capacity, and then training this network using large sets of labeled examples [27].

There are two main methods for reconstructing face images from templates, based on either multidimensional scaling (MDS) [10] or radial basis function (RBF) regression [9]. However, these methods have only been evaluated using shallow templates[8]. The MDS-based method [10] uses a set of face images to generate a similarity score matrix using the target face recognition system, and then finds an affine space in which face images can approximate the original similarity matrix. Once the affine space has been found, a set of similarities is obtained from the target face recognition system by matching the target template and the test face images. The affine representation of the target template is estimated using these similarities, which is then mapped back to the target face image.

The RBF-regression-based method [9] directly maps target templates to whitened eigenfaces and then inverts them to the face image. Given a set of bases in the template space, (multi-quadric) RBF regression [9] generates vectors consisting of distances from the face representations to the given basis, and then maps these vectors to the whitened eigenfaces using least squares regression.

Both of these reconstruction methods provide limited capacity for modeling complex mapping between face images and deep templates. The MDS-based method [10] models the mapping between face images and face templates linearly. In contrast, the RBF-regression-based method [9] models non-linearity between face images and face templates using a multi-quadric kernel.

2.2 D-CNN for Generating Face Images

A typical D-CNN is a cascade of multiple de-convolutional operators, each consisting of one or more de-convolution, activation (non-linear), and up-sampling layer(s) [30], [31]. Convolutional layers produce convolutions of input signals. Conversely, de-convolutional layers produce output signals that can be convolved to the input signals of the corresponding convolutional network. D-CNNs have been shown to be capable of generating face images from dynamically generated small-size vectors (a random vector or hidden representation) [34], [35], [36]. The variational auto-encoder [35] uses a D-CNN to map hidden representations (dynamically) generated from a co-training encoder back to the corresponding face images. The deep convolutional generative adversarial network (DCGAN) [34] uses a D-CNN as a generative model to map a random vector to a face image. The attribute2Image [36] uses a D-CNN to map a random vector together with an attribute descriptor to a face image with specific attributes (e.g., hair color, gender, or age).

3 Proposed Template Security Study

An overview of our security study for deep-template-based face recognition systems under image reconstruction attack is shown in Fig. 3; the normal and image reconstruction attack flows are shown as black solid and red dotted lines, respectively. In this section, we first describe the image reconstruction attack scenario using an adversarial machine learning framework [37]. The reconstruction of face images from deep templates using a D-CNN and the corresponding training strategy and implementation are then detailed.

3.1 Image Reconstruction Attack Scenario

The adversarial machine learning framework [37] categorizes biometric attack scenarios from four perspectives: an adversary's goal, knowledge, capability, and attack strategy. Given a deep-template-based face recognition system operating in a verification mode, our image reconstruction attack scenario using the adversarial machine learning framework is detailed as follows.

- *Adversary's goal:* The attacker aims to impersonate the target subject in the target face recognition system, violating the system integrity.
- *Adversary's knowledge:* The attacker is assumed to know the following information. (a) The templates $\boldsymbol{y}_t$ of the target subjects. These can be obtained via

8. Shallow templates refer to templates that were not extracted using a deep network.

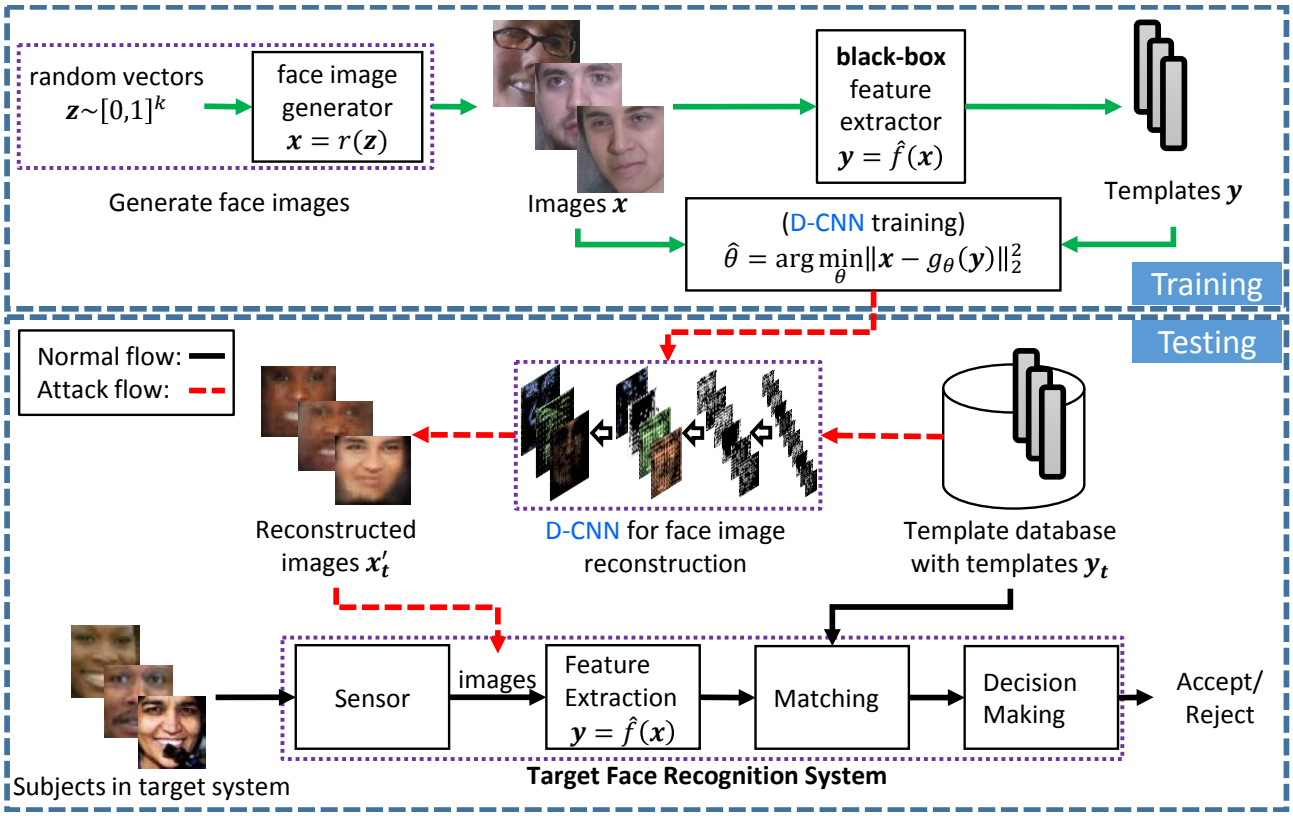

Fig. 3. An overview of our template security study of deep network based face recognition systems under image reconstruction attack.

template database leakage or an insider attack. (b) The *black-box* feature extractor $\boldsymbol{y} = \hat{f}(\boldsymbol{x})$ of the target face recognition system. This can potentially be obtained by purchasing the target face recognition system's SDK. The attacker has no information about target subjects nor their enrollment environments. Therefore, no face images enrolled in the target system can be used in the attack.

- *Adversary's capability:* (a) Ideally, the attacker should only be permitted to present fake faces (2D photographs or 3D face masks) to the face sensor during verification. In the present study, to simplify, the attacker was assumed to be able to insert face images to the feature extractor as if the images were captured by the face sensor. Note that the inserted images coud also be used to create fake faces in actual attacks. (b) The identity decision for each query is available to the attacker. However, the similarity score of each query is unavailable to the attacker. (e) Only a small number of trials (for example, < 5) are permitted for the recognition of a target subject.
- *Attack strategy:* Under these assumptions, the attacker can infer face images $\boldsymbol{x}_t$ from the target templates $\boldsymbol{y}_t$ using a reconstruction model $\boldsymbol{x}_t = g_{\boldsymbol{\theta}}(\boldsymbol{y}_t)$ and insert reconstructed images as queries to access the target face recognition system. The parameter $\boldsymbol{\theta}$ of the reconstruction model $g_{\boldsymbol{\theta}}(\cdot)$ can be learned using public domain face images.

3.2 D-CNN for Face Image Reconstruction

Our D-CNN-based face image reconstruction model followed the architecture guidelines proposed by Radford et al. [34]. As shown in Fig. 4, the D-CNN used in the present study is a cascade of five de-convolutional network operators, which are comprised of a de-convolutional layer [30], [31], a batch normalization layer [38], and a ReLU activation [39] (tanh activation for the fifth layer) layer. The input and output sizes of D-CNNs can be adjusted based on the feature extractor of the target face recognition system. In the present study, Openface[9] [40], was chosen as the target face recognition engine. Openface is an open source implementation of FaceNet [12]. Consequently, the D-CNN input is a feature vector of size 128 and the output is a tensor of size $96 \times 96 \times 3$. The main advantage of using a D-CNN is its rich model capacity for modeling complex mapping between face images and deep templates.

The de-convolutional layer maps an abstract signal to a less abstract one by expanding convolutions to their original signal. Thus, a D-CNN with stacked de-convolutional layers expands highly abstracted templates back to the corresponding face images hierarchically. Taking the deep template extracted from the leftmost image in Fig. 4 as input, a visualization of the corresponding activations of the third and the fourth de-convolutional layers in our trained D-CNN are shown in Fig. 5. In visualizing the third de-convolutional layer (Fig. 5a), most of the activated channels are shown as thumbnails of whole or partial face images containing either little or no detail. The details of the

9. https://cmusatyalab.github.io/openface/

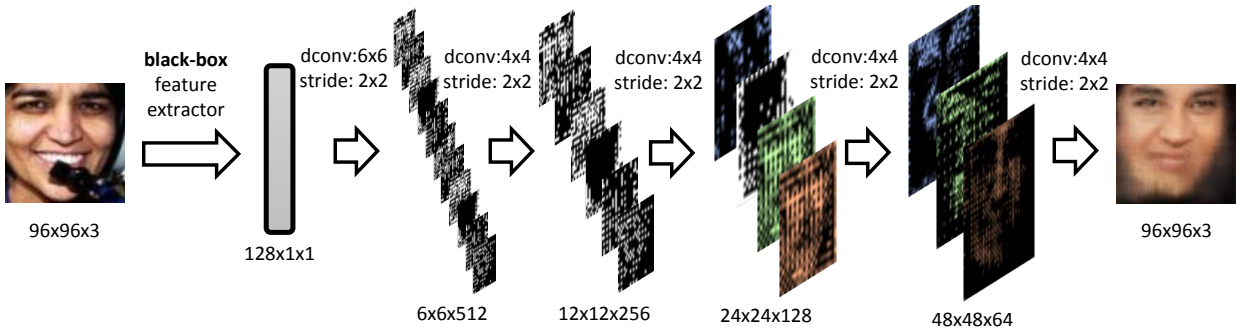

Fig. 4. The proposed de-convolutional neural network (D-CNN) for reconstructing face images from the corresponding face templates. The numbers (w $\times$ h $\times$ c) below each layer denote its width, height, and number of channels, respectively. The network architecture is identical to the generative model in a DCGAN [34], except for the size of the input and output.

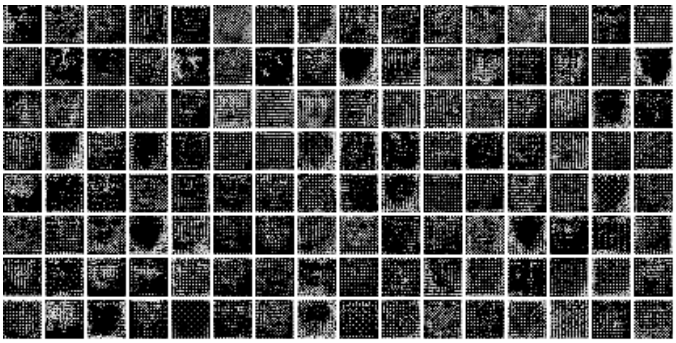

(a) Visualization of activations of the third de-convolutional layer

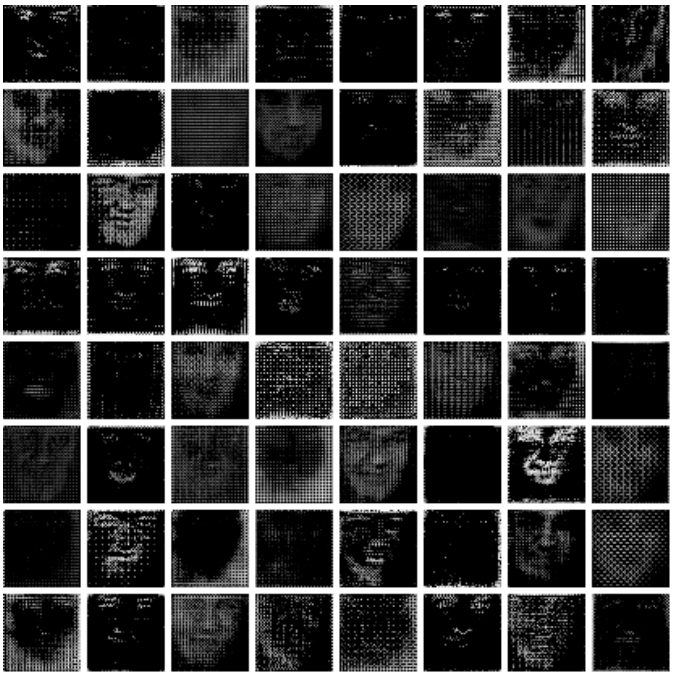

(b) Visualization of activations of the fourth de-convolutional layer

Fig. 5. Visualizations of activations of (a) 128 (8×16) channels in the third de-convolutional layer, and (b) 64 (8×8) channels in the fourth de-convolutional layer. The face image used for extracting the deep template and corresponding output face image are the leftmost and rightmost images in Fig. 4.

activated channels in the third de-convolutional layer are expanded upon in the fourth de-convolutional layer (Fig. 5b). For example, some images contain the shape of the whole face, and others contain outlines or details of the eyes, nose, and mouth. Finally, these activations are expanded upon to produce the reconstructed face image (the rightmost image in Fig. 4).

3.3 Generating Face Images for Training D-CNN

To accomplish image reconstruction attack on a face recognition system without knowledge of the target subject population, the reconstruction D-CNN should be able to accurately reconstruct face images with input templates extracted from face images of different subjects. Let $g_{\boldsymbol{\theta}}(\cdot)$ denote a D-CNN with parameter $\boldsymbol{\theta}$, $\boldsymbol{x}$ denote an input face image, and $p_{\boldsymbol{x}}(\boldsymbol{x})$ denote the probability density function (pdf) of image $\boldsymbol{x}$. The objective function for training a D-CNN can be formulated as

$$\arg\min_{\boldsymbol{\theta}} \mathcal{L}(\boldsymbol{\theta}) = \arg\min_{\boldsymbol{\theta}} \int \mathcal{R}(\boldsymbol{x}, \boldsymbol{\theta}) p_{\boldsymbol{x}}(\boldsymbol{x}) d\boldsymbol{x} \qquad (1)$$

where $\mathcal{R}(\boldsymbol{x}, \boldsymbol{\theta}) = \left\| \boldsymbol{x} - g_{\boldsymbol{\theta}}(\hat{f}(\boldsymbol{x})) \right\|_2^2$ denotes the reconstruction loss between image $\boldsymbol{x}$ and its reconstruction, and $\hat{f}(\cdot)$ denotes a *black-box* feature extractor. Since there are no explicit methods for estimating $p_{\boldsymbol{x}}(\boldsymbol{x})$, we cannot sample face images from $p_{\boldsymbol{x}}(\boldsymbol{x})$. The common approach is to collect a large-scale face dataset and approximate the loss function $\mathcal{L}(\boldsymbol{\theta})$ in Eq. (1) as:

$$\mathcal{L}(\boldsymbol{\theta}) = \frac{1}{N} \sum_{i}^{N} \mathcal{R}(\boldsymbol{x}_i, \boldsymbol{\theta}) \qquad (2)$$

where N denotes the number of collected face images and $\boldsymbol{x}_i$ denotes the i-th training image. This approximation is optimal if, and only if, N is very large. In practice, this is not feasible because of the huge time and cost associated with data collection.

To train a highly generalizable D-CNN for reconstructing face images from their deep templates, a large number of face images are required. Ideally, these face images should come from many different subjects because deep face templates of the same subject are very similar and can be regarded as either single exemplar or under large intra-user variations, a small set of exemplars in the training of D-CNN. However, current large-scale face datasets

(such as VGG-Face [22], CASIA-Webface [41], and Multi-PIE [42]) were primarily collected for training or evaluating face recognition algorithms. Hence, they either contain an insufficient number of images (for example, 494K images in CASIA-Webface) or an insufficient number of subjects (for instance, 2,622 subjects in VGG-Face and 337 subjects in Multi-PIE) for training a reconstruction D-CNN.

Instead of collecting a large face image dataset for training, we augmented current publicly available datasets. A straightforward way to augment a face dataset is to estimate the distribution of face images and then sample the resulting distribution. However, as face images generally consist of very large number of pixels, there is no efficient method to model the joint distribution of these pixels. Therefore, we introduced a generator $\boldsymbol{x} = r(\boldsymbol{z})$ capable of generating a face image $\boldsymbol{x}$ from a vector $\boldsymbol{z}$ with a given distribution. Assuming that $r(\boldsymbol{z})$ is one-to-one and smooth, the face images can be sampled by sampling $\boldsymbol{z}$. The loss function $\mathcal{L}(\boldsymbol{\theta})$ in Eq. (1) can then be approximated as follows:

$$\begin{aligned}\mathcal{L}(\boldsymbol{\theta}) &= \int \mathcal{R}(\boldsymbol{x}, \boldsymbol{\theta}) p_{\boldsymbol{x}}(\boldsymbol{x}) d\boldsymbol{x} \\ &= \int \mathcal{R}(r(\boldsymbol{z}), \boldsymbol{\theta}) p_{\boldsymbol{z}}(\boldsymbol{z}) d\boldsymbol{z}\end{aligned} \tag{3}$$

where $p_{\boldsymbol{z}}(\boldsymbol{z})$ denotes the pdf of variable $\boldsymbol{z}$. Using the *change of variables* method [43], [44], it is easy to show that $p_{\boldsymbol{z}}(\boldsymbol{z})$ and $r(\boldsymbol{z})$ should satisfy the following equation.

$$p_{\boldsymbol{z}}(\boldsymbol{z}) = p_{\boldsymbol{x}}(r(\boldsymbol{z})) \left| \det \left(\frac{d\boldsymbol{x}}{d\boldsymbol{z}} \right) \right| \tag{4}$$

Suppose a face image $\boldsymbol{x} \in \mathbb{R}^{h \times w \times c}$ of height h, width w, and with c channels can be represented by a real vector $\boldsymbol{b} = \{b_1, \cdots, b_k\} \in \mathbb{R}^k$ in a manifold space with $h \times w \times c \gg k$. It can then be shown that there exists a generator function $\boldsymbol{b'} = \hat{r}(\boldsymbol{z})$ that generates $\boldsymbol{b'}$ with a distribution identical to that of $\boldsymbol{b}$, where $\boldsymbol{b}$ can be arbitrarily distributed and $\boldsymbol{z} \in [0, 1]^k$ is uniformly distributed (see Appendix).

To train the D-CNN in the present study, we used the generative model of a DCGAN [34] as our face generator $r(\cdot)$. This model can generate face images from vectors $\boldsymbol{z}$ that satisfy a uniform distribution. Specifically, DCGAN generates face images $r(\boldsymbol{z})$ with a distribution approximated to that of real face images $\boldsymbol{x}$. It can be shown empirically that a DCGAN can generate face images of unseen subjects with different intra-subject variations. By using adversarial learning, the DCGAN is able to generate face images that are classified as real face images by a co-trained real/fake face image discriminator. Besides, the intra-subject variations generated using a DCGAN can be controlled by performing arithmetic operations in the random input space [34].

3.4 Implementation Details

3.4.1 Network Architecture

The de-convolutional layers of D-CNN shown in Fig. 4 have a kernel size of 4×4 (6×6 in the first layer) and a stride size of 2×2. The 2×2 stride of the de-convolutional layers is used for up-sampling. Therefore, there are no explicit up-sampling layers. The five de-convolutional layers have 512, 256, 128, 64, and 3 channels, respectively. This network architecture is identical to the generative model of a DCGAN [34], except for the kernel size in the first de-convolutional layer and the input and output sizes.

Algorithm 1 D-CNN training using a face image generator with batch gradient descent

Input:
Distribution $p_{\boldsymbol{z}}(\boldsymbol{z})$ of random variable $\boldsymbol{z}$
Face image generator $\boldsymbol{x} = r(\boldsymbol{z})$
Feature extractor (black-box) $\boldsymbol{y} = \hat{f}(\boldsymbol{x})$
Maximum number of batches n
Batch size s
Output: Feature decoder $\tilde{\boldsymbol{x}} = g_{\boldsymbol{\theta}}(\boldsymbol{y})$
$i \leftarrow 1$
while $i \leq n$ **do**
  $Z \leftarrow s$ random vectors $\boldsymbol{z}$ sampled from $p_{\boldsymbol{z}}(\boldsymbol{z})$
  $X \leftarrow s$ face images $\boldsymbol{x}$ generated from Z using $r(\boldsymbol{z})$
  $Y \leftarrow s$ face features $\boldsymbol{y}$ extracted from X using $\hat{f}(\boldsymbol{x})$
  Update parameter $\boldsymbol{\theta}$ of $g_{\boldsymbol{\theta}}(\boldsymbol{y})$ with (Y, X) using batch gradient descent.
  $i \leftarrow i + 1$
end while

The DCGAN [34] used in this study consist of a generative model and a discriminative model. The generative model was the same as a D-CNN with an input vector size of 100. The discriminative model is a cascade of five convolutional operators, which are comprised of a convolutional layer with a kernel size of 4×4 (6×6 in the last layer) and a stride size of 2×2, a batch normalization layer, and a ReLU (excepting the final operator) activation layer. The five convolutional layers consisted of 64, 128, 256, 512, and 1 channels, respectively. A logistic regression was used for the loss layer of the discriminative model.

3.4.2 Training Details

To train our D-CNN to reconstruct face images from deep templates, we first trained a DCGAN to generate face images. These generated images were then used for training. The DCGAN was trained according to the method detailed in [34]. After pre-training, random vectors $\boldsymbol{z}$ were sampled from a uniform distribution. Face images were generated from $\boldsymbol{z}$ and the corresponding face templates were extracted. The training algorithm was based on batch gradient descent optimization (Algorithm 1). This training strategy was used to minimize the loss function $\mathcal{L}(\boldsymbol{\theta})$ in Eq. (3), which approximates the loss function in Eq. (1).

The pixel values in the output image were normalized to $[-1, 1]$, and the batch size set to 64. The weights were initialized using a normal distribution with zero mean and a standard deviation of 0.02. Adam [45] was used for optimization, with a learning rate of 2×10^{-4} and an exponential decay rate, where $\beta_1 = 0.5$ and $\beta_2 = 0.999$.

4 Experimental Results

4.1 Database and Experimental Setting

The vulnerabilities of deep templates under image reconstruction attacks were studied with our proposed reconstruction model, using three large-scale face datasets for training and two different benchmark datasets for testing. The training datasets consisted of two unconstrained

(a) VGG-Face (b) CASIA-Webface (c) Multi-PIE (d) LFW (e) FRGC v2.0

Fig. 6. Example face images from the training datasets: (a) VGG-Face (1.89M images) [22], (b) CASIA-Webface (414K images) [41], and (c) Multi-PIE (151K images, only three camera views were used, including '14_0', '05_0' and '05_1', respectively) [42]. Example face images from the testing datasets: (d) LFW (13,233 images) [24], [48], and (e) FRGC v2.0 (16,028 images in the target set of Experiment 1) [47].

datasets, (VGG-Face [22] and CASIA-Webface [41]), and one constrained dataset (Multi-PIE [42]).

- **VGG-Face** [22] comprises of 2.6 million face images from 2,622 subjects. In total, 1,890,068 trainable images were obtained by downloading the provided image links and then aligning the faces with landmarks detected using Dlib[10] [11].
- **CASIA-Webface** [41] consists of 494,414 face images from 10,575 subjects. After preprocessing (detection and alignment), we obtained 413,958 training images with detectable face landmarks.
- **Multi-PIE** [42]. We used 150,760 frontal images from this dataset (3 camera views, with labels '14_0', '05_0', and '05_1', respectively), from 337 subjects. The landmarks used in this study were obtained from [46].

Two testing datasets were used, including one unconstrained dataset (LFW [24]) and one constrained dataset (Face Recognition Grand Challenge (FRGC) v2.0 [47]).

- **LFW** [24] consists of 13,233 images of 5,749 subjects obtained from the Web.
- **FRGC v2.0** [47] consists of 50,000 frontal images of 4,003 subjects with two different facial expressions (smiling and neutral), taken under different illumination conditions. A total of 16,028 images of 466 subjects (as specified in the target set of Experiment 1 of FRGC v2.0 [47]) were used.

The face images were aligned relative to the eyes and nose and then cropped to 96×96 pixels [40]. Instead of aligning images from the LFW dataset, we used the pre-aligned deep funneled version [48]. Fig. 6 shows example images from these five datasets.

To determine the effectiveness of the proposed generator-based training strategy using a DCGAN [34], we compared D-CNNs trained using the proposed strategy

10. https://github.com/davisking/dlib

11. All of the face landmarks in this work were detected using Dlib, unless otherwise stated.

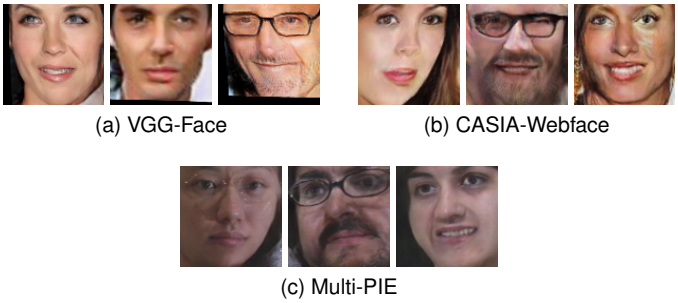

(a) VGG-Face (b) CASIA-Webface (c) Multi-PIE

Fig. 7. Sample images generated from face generators trained on (a) VGG-Face, (b) CASIA-Webface, and (c) Multi-PIE.

with those trained using typical strategies (in which face images from a specific training dataset were used directly). We augmented three training face datasets using face images generated by a DCGAN. The VGG-Face, CASIA-Webface, and Multi-PIE datasets were augmented from 1.89M, 414K, and 151K images to 128M, 56M, and 26M images, respectively. Examples of images generated using our trained face image generator are shown in Fig. 7. In addition, the proposed D-CNN based reconstruction method was compared with a state-of-the-art RBF-regression-based method [9]. In contrast to the D-CNN based method, the RBF regression model of [9] used the same dataset for training and testing (either LFW or FRGC v2.0). Therefore, the RBF-regression-based reconstruction method was expected to have better reconstruction accuracy than the proposed D-CNN method. The MDS-based method [10] was not compared here because it is a linear model and was not as good as the RBF-regression-based method [9]. Table 2 summarizes seven comparison models used in this study for deep template inversion.

In addition to images obtained from these seven reconstruction models, we also used the **Fused** results, which were obtained by fusing the decisions from the VGG-Gen, CASIA-Gen, and Multi-PIE-Gen models. This can be regarded as a three-trial attack, which typically combines the most accurate results of these generator-based models. Most authentication systems (such as ATMs or smart-phones) accept three attempts before locking out the customer.

We used face templates extracted using FaceNet [12], one of the most accurate CNN models for face recognition currently available. To ensure the face reconstruction scenario was realistic, we used an open-source implementation (Openface [40]) without any modifications (model *nn4.small2.v1*).

Examples of the most accurately reconstructed face images are shown in Fig. 8. The leftmost column shows the original images, and the remaining columns show the images reconstructed using the seven reconstruction models. For the RBF model, every image in the testing datasets (LFW and FRGC v2.0) has 10 different reconstructed images that can be created using the 10 cross-validation trials in the BLUFR protocol [12] [49]. The RBF-reconstructed images shown here are those with the highest similarity scores among these 10 different reconstructions. Each row shows

12. http://www.cbsr.ia.ac.cn/users/scliao/projects/blufr/

TABLE 2
Deep template face image reconstruction models for comparison

Model	Training Dataset	Testing Dataset	Training and Testing Process
VGG-Gen	VGG-Face	LFW, FRGC v2.0	Train a DCGAN using the training dataset, and then use face images generated from the pre-trained DCGAN for training the target D-CNN. Test the trained D-CNN using testing datasets.
CASIA-Gen	CASIA-Webface		
Multi-PIE-Gen	Multi-PIE		
VGG-Raw	VGG-Face		Directly train the target D-CNN using face images from the training dataset, and then test the trained D-CNN using testing datasets.
CASIA-Raw	CASIA-Webface		
Multi-PIE-Raw	Multi-PIE		
RBF [9]	LFW	LFW	Train and test the RBF regression based method using the training and testing images specified in the evaluation protocol.
	FRGC v2.0	FRGC v2.0	

the most accurate reconstruction using different models. The number below each image is the similarity score between the original and reconstructed images. The similarity scores were calculated using the cosine similarity, the range of which is $[-1, 1]$. All of the most accurately reconstructed face images are frontal images with open eyes and either a smiling or neutral expression.

The models trained using images generated by the three face image generators (VGG-Gen, CASIA-Gen, and Multi-PIE-Gen) produced more accurate reconstructions than those trained with the original training datasets (VGG-Raw, CASIA-Raw, and Multi-PIE-Raw). The difference was more pronounced for small training datasets (CASIA-Webface and Multi-PIE). The reconstructed images from VGG-Gen were only slightly more accurate than those reconstructed from VGG-Raw with about 1.89M images. However, the CASIA-Raw and Multi-PIE-Raw datasets contained a relatively small number of training images, resulting in the poor generalizability of the trained reconstruction models. Furthermore, the colors of the face images reconstructed from the VGG and CASIA models appeared more realistic than those reconstructed from the Multi-PIE models. The images in Multi-PIE were collected indoors under controlled conditions. In contrast, VGG-Face and CASIA-Webface contained images of a large number of subjects captured in diverse conditions. The face images reconstructed from the RBF model in [9] appeared more similar to the original images in terms of color and shape because i) the training and testing images came from the same dataset and ii) the images shown herein are the most accurate, based on tenfold cross-validation.

TABLE 3
TARs (%) of type-I attacks on LFW for different image reconstruction methods, where "Original" denotes results based on the original images and "Fused" denotes a decision-level fusion of VGG-Gen, CASIA-Gen, and Multi-PIE-Gen reconstructions. The other methods are described in Table 2.

Method	FAR=0.1%	FAR=1.0%
Original	100	100
VGG-Gen	60.23	89.20
VGG-Raw	48.53	79.58
CASIA-Gen	68.11	92.22
CASIA-Raw	22.58	55.30
Multi-PIE-Gen	45.26	75.89
Multi-PIE-Raw	9.93	32.81
Fused	85.48	98.80
RBF [9]	22.08	53.55

TABLE 4
TARs (%) of type-II attacks on LFW for different image reconstruction methods, where "Original" denotes the results based on the original images and "Fused" denotes a decision-level fusion of VGG-Gen, CASIA-Gen, and Multi-PIE-Gen reconstructions. The other methods are described in Table 2.

Method	FAR=0.1%	FAR=1.0%
Original	24.87	58.55
VGG-Gen	4.80	27.23
VGG-Raw	7.70	28.69
CASIA-Gen	8.63	31.04
CASIA-Raw	4.27	18.70
Multi-PIE-Gen	4.41	23.35
Multi-PIE-Raw	1.05	8.76
Fused	14.71	46.88
RBF [9]	4.69	22.84

4.2 Verification Under Image Reconstruction Attack

We quantitatively evaluated the template security of the target face recognition system (FaceNet) under type-I and type-II image reconstruction attacks. The evaluation metric was face verification using the BLUFR protocol [49]. The impostor scores obtained from the original face images were used in both of the attacks to demonstrate the efficacy of the reconstructed face images. The genuine scores in the type-I attack were obtained by comparing the reconstructed images against the original images. The genuine scores in the type-II attack were obtained by substituting one of the original images in a genuine comparison (image pair) with the corresponding reconstructed image. For benchmarking, we report the "Original" results based on original face images. Every genuine score of "Original" in type-I attack was obtained by comparing two identical original images. The genuine scores of "Original" in type-II attack were obtained by the genuine comparisons specified in BLUFR protocol. The BLUFR protocol uses tenfold cross validation; the performance reported here is the 'lowest', namely $(\mu - \sigma)$, where μ and σ denote the mean and standard deviation of the reconstruction performance obtained from the 10 trials, respectively.

4.2.1 Performance on LFW

In each evaluation trial of the BLUFR protocol [49] for LFW [24], there is an average of 46,960,863 impostor comparisons. The average number of testing images is 9,708. Hence, there are 9,708 genuine comparisons in a type-I attack on LFW. The average number of genuine comparisons in a type-II

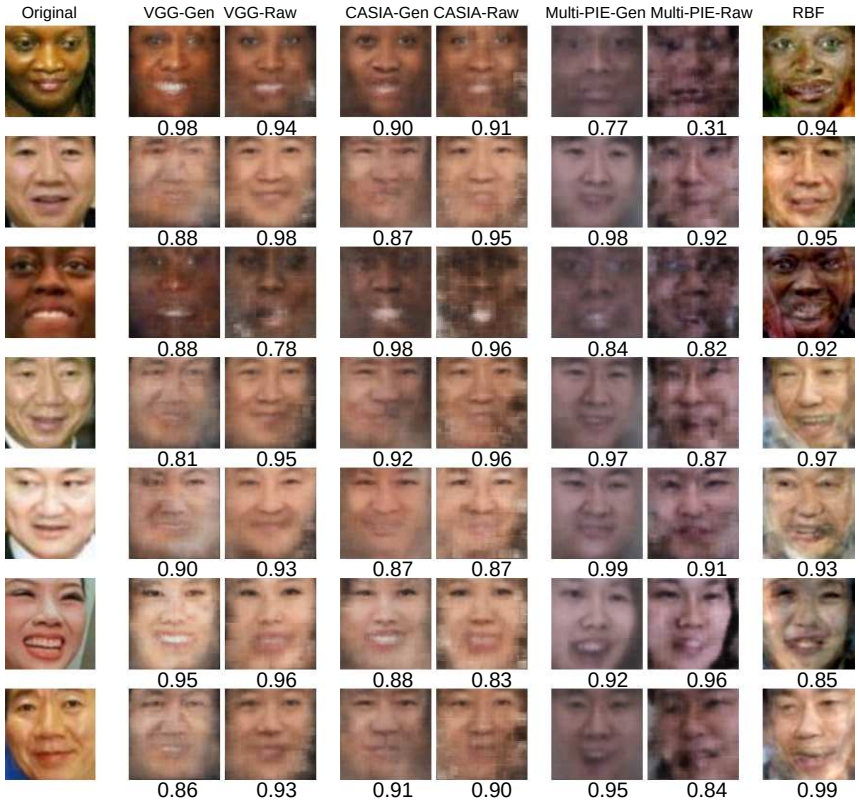

(a) LFW

(b) FRGC v2.0

Fig. 8. The most accurate reconstructed face images from (a) LFW and (b) FRGC v2.0. The original images are shown in the first column. Each column denotes the model used for reconstruction. Each row shows the most accurate reconstruction (highest similarity score with the original image) using different reconstruction models. The number below each reconstructed image shows the similarity score between the reconstructed image and the original image. The scores were calculated using the cosine similarity, ranging from -1 to 1. The verification thresholds on LFW and FRGC v2.0 were 0.78 and 0.94, respectively, at FAR=0.1%, and 0.66 and 0.90, respectively, at FAR=1.0%.

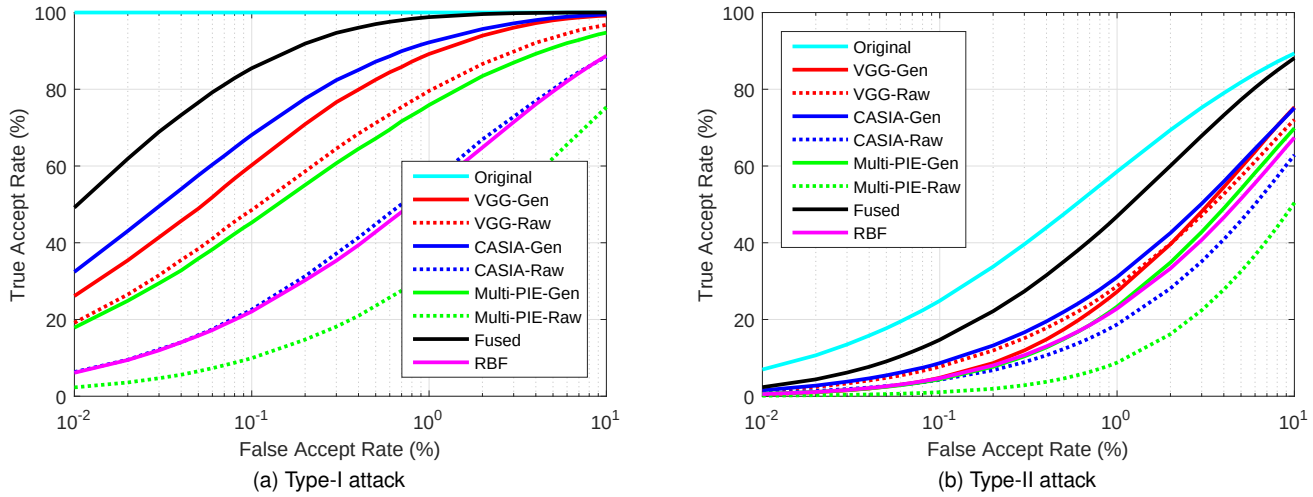

Fig. 9. ROC curves of (a) type-I and (b) type-II attacks using different reconstruction models on LFW.

Fig. 10. Examples of unsuccessful reconstructions of face images in the LFW dataset as a result of (a) large pose variations, (b) exaggerated expressions, (c) occlusion or the presence of sunglasses, or (d) incorrect alignment. The columns denote the models used for reconstruction. The number below each reconstructed image is the similarity score between the original face image and the corresponding reconstruction. The scores were calculated using the cosine similarity, ranging from -1 to 1. The verification thresholds were 0.78 and 0.66 at FAR=0.1 and 1.0%, respectively.

attack on LFW is 156,915; this is the average number of genuine comparisons specified in the BLUFR protocol.

The receiver operator characteristic (ROC) curves of type-I and type-II attacks on LFW are shown in Fig. 9. Tables 3 and 4 show the corresponding values of TAR at FAR=0.1% and FAR=1.0%, respectively. The ROC curve of "Original" base on the original face images. It is always 100% for the type-I attack (Fig. 9a) because the corresponding genuine similarity scores are obtained by comparing two identical images. In the type-II attack (Fig. 9b), "Original" is the system performance with BLUFR protocol [49] based on original images.

For both type-I and type-II attacks, the models trained using the proposed strategy (VGG-Gen, CASIA-Gen, and Multi-PIE-Gen) generally outperformed RBF and the models trained with the non-augmented datasets (VGG-Raw, CASIA-Raw, and Multi-PIE-Raw). Moreover, in a type-II attack, VGG-Gen outperformed VGG-Raw by 2.0% FAR. Multi-PIE-Raw model demonstrated the worst reconstruction performance because the Multi-PIE dataset consists of only 337 subjects, with limited intra-subject variations. In the type-I attack, the fusion of VGG-Gen, CASIA-Gen, and Multi-PIE-Gen model results achieved a TAR of 85.48% (98.80%) at FAR=0.1% (FAR=1.0%). This implies that attackers had approximately an 85% (or 99% at FAR=1.0%) chance of accessing the system within three attempts using a leaked template.

Examples of unsuccessful reconstructions of LFW images are shown in Fig. 10. These unsuccessful reconstructions exhibited four major characteristics: large pose variations (Fig. 10a), exaggerated expressions (Fig. 10b), occlusions or the presence of sunglasses (Fig. 10c), and incorrect alignment (Fig. 10d).

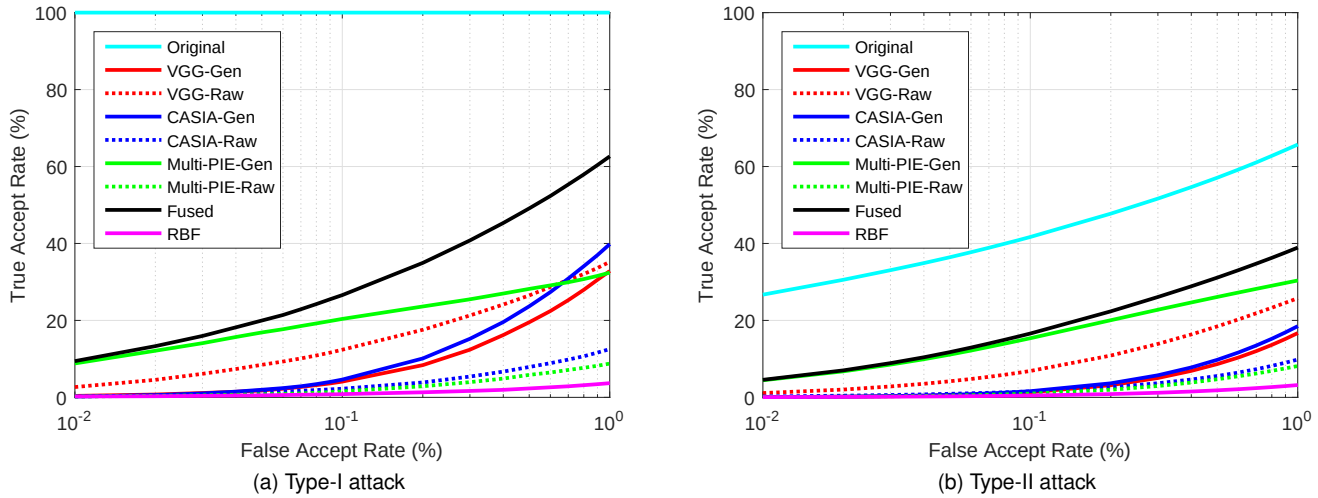

Fig. 11. ROC curves of (a) type-I and (b) type-II attacks using different reconstruction models on FRGC v2.0.

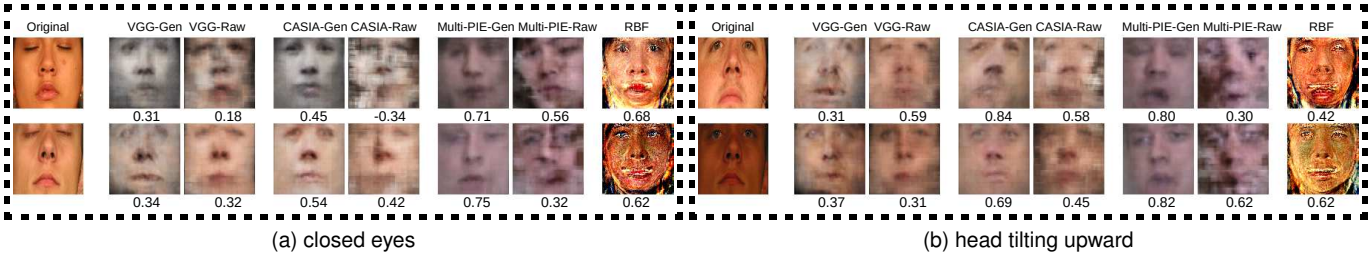

Fig. 12. Examples of unsuccessful reconstructions of face images in the FRGC v2.0 dataset as a result of (a) closed eyes and (b) head tilting upward. The original images from FRGC v2.0 are shown in the first column. The remaining columns show the reconstructions obtained using the VGG-Gen, VGG-Raw, CASIA-Gen, CASIA-Raw, Multi-PIE-Gen, Multi-PIE-Raw, and RBF methods, respectively. The similarity scores shown below each reconstructed image were calculated using the cosine similarity, [-1,1], between the original and reconstructed images. The verification thresholds of the similarity scores were 0.94 and 0.90 at FAR=0.1 and 1.0%, respectively.

TABLE 5
TARs (%) of type-I attacks on FRGC v2.0 for different image reconstruction methods, where "Original" denotes results based on the original images and "Fused" denotes a decision-level fusion of VGG-Gen, CASIA-Gen, and Multi-PIE-Gen reconstructions. The other methods are described in Table 2.

Methods	FAR = 0.1%	FAR = 1.0%
Original	100	100
VGG-Gen	4.10	32.84
VGG-Raw	12.38	35.21
CASIA-Gen	4.62	39.81
CASIA-Raw	2.25	12.54
Multi-PIE-Gen	20.39	32.42
Multi-PIE-Raw	1.57	8.78
Fused	26.58	62.63
RBF [9]	0.84	3.69

TABLE 6
TARs (%) of type-II attacks on FRGC v2.0 for different image reconstruction methods, where "Original" results based on the original images and "Fused" denotes a decision-level fusion of VGG-Gen, CASIA-Gen, and Multi-PIE-Gen reconstructions. The other methods are described in Table 2.

Methods	FAR = 0.1%	FAR = 1.0%
Original	41.69	65.71
VGG-Gen	1.33	16.71
VGG-Raw	6.86	25.76
CASIA-Gen	1.61	18.50
CASIA-Raw	1.56	9.83
Multi-PIE-Gen	15.37	30.38
Multi-PIE-Raw	0.98	8.15
Fused	16.60	38.92
RBF [9]	0.48	3.20

4.2.2 Performance on FRGC v2.0

Each evaluation trial of the BLUFR protocol [49] for FRGC v2.0 [47] consisted of an average of 76,368,176 impostor comparisons. There was an average of 12,384 testing images. Hence, there were 12,384 genuine comparisons in a type-I attack. There was an average of 307,360 genuine comparisons in a type-II attack; this was the average number of genuine comparisons according to the BLUFR protocol.

The ROC curves of type-I and type-II attacks on FRGC v2.0 are shown in Fig. 11. The TAR values at FAR=0.1 and FAR=1.0% are shown in Tables 5 and 6, respectively. The TAR values (Tables 3, 4, 5, and 6) and ROC plots (Figs. 9 and 11) for LFW and FRGC v2.0 cannot be directly compared, as the thresholds for LFW and FRGC v2.0 differ (e.g., the thresholds at FAR=0.1% are 0.78 and 0.94 for LFW and FRGC v2.0, respectively). The similarity threshold values

were calculated based on the impostor distributions of the LFW and FRGC v2.0 databases. As in the LFW results, the curve "Original" for the type-I attack (Fig. 11a) is always 100%. In the type-II attack (Fig. 11b), "Original" is the system performance with BLUFR protocol [49] based on original images. Significant improvements by using the augmented datasets (CASIA-Gen and Multi-PIE-Gen) were observed, compared with CASIA-Raw and Multi-PIE-Raw, for both the type-I and type-II attacks. The performance of VGG-Gen was not as good as that of VGG-Raw. However, the VGG-Gen reconstructions with similarity scores greater than the thresholds for FAR=0.1% and 1.0% were based on 167 and 359 subjects, respectively. The equivalent VGG-Raw reconstructions were based on 159 and 319 subjects, respectively. This implies that VGG-Gen was more generalizable than VGG-Raw in terms of different subjects. All of the D-CNN models outperformed the RBF model. In the type-I attack, the fused decision (based on VGG-Gen, CASIA-Gen, and Multi-PIE-Gen) achieved a TAR of 26.58% (62.63%) at FAR=0.1% (FAR=1.0%). This implies that attackers had a 27% (63%) chance of accessing the system at FAR=0.1% (1.0%) within three trials using a leaked template.

Unsuccessful reconstructions of face images from FRGC v2.0 are shown in Fig. 12. Similar to the unsuccessful reconstructions on the LFW dataset, the unsuccessful reconstructions of FRGC v2.0 images contained relatively large variations, such as closed eyes (Fig. 12a) and head tilted upward (Fig. 12b).

4.3 Computation Time

We implemented the D-CNN on an NVIDIA GeForce GTX TITAN X with Maxwell (GPU) and an Intel(R) Xeon(R) E5-2680 v3 @ 2.50 GHz (CPU) with MXNET[13] [50]. The average time to reconstruct a single face image was 0.204 s using the CPU, and 0.693 μs using the GPU.

To ensure a fair comparison, the number of batch training iterations was identical for the D-CNNs trained on generated and raw face images; each batch consisted of 64 face images. The VGG-Gen and VGG-Raw networks were trained with around 2M batches. The CASIA-Gen and CASIA-Raw networks were trained with around 900K batches. The Multi-PIE-Gen and Multi-PIE-Raw networks were trained with around 400K batches.

5 Conclusions and Future Work

We investigated the security of deep templates by studying the reconstruction of face images via the inversion of their deep templates. A D-CNN-based method for reconstructing face images from the corresponding deep templates and a strategy for training highly generalizable D-CNNs were developed. Experimental results indicated that the proposed D-CNN-based reconstruction method outperformed RBF-regression-based reconstruction in terms of attack success rates. Furthermore, models trained using the proposed generator-based training strategy outperformed equivalent models trained using a conventional strategy. The reconstructions were shown to be effective, and the average time taken to reconstruct a single image was 0.204 s using a CPU (Intel(R) Xeon(R) E5-2680 v3 @ 2.50 GHz) and 0.693 μs using a GPU (NVIDIA GeForce GTX TITAN X with Maxwell).

This study revealed a potential security issue resulting from template leakage in state-of-the-art face recognition systems, particularly for systems based on deep templates. Therefore, we encourage the use of template protection schemes detailed in [51], [52], [53], [54], [55] to prevent the leakage of face templates. However, template protection methods are imperfect because of trade-offs between discriminability and invertibility [51]. To overcome these limitations, anti-spoofing techniques [6], [7], [8] are suggested for increasing system security. Our future research goals are as follows: (*i*) to devise a more effective reconstruction algorithm by considering the significance of pixels in different face regions; (*ii*) to theoretically analyze a face image generator to determine the completeness property for the given input space, and (*iii*) to study cross-system attacks using face images reconstructed from the templates of a given face recognition system to access a different face recognition system.

Appendix

Proof of the Existence of a Face Image Generator

Suppose a face image $\boldsymbol{x} \in \mathbb{R}^{h\times w\times c}$ of height h, width w, and c channels can be represented by a real vector $\boldsymbol{b} = \{b_1, \cdots, b_k\} \in \mathbb{R}^k$ in a manifold space with $h \times w \times c \gg k$, where $b_i \sim \mathcal{F}_{b_i}, i \in [1, k]$ and $\mathcal{F}_{b_i}$ is the cumulative distribution function of b_i. The covariance matrix of $\boldsymbol{b}$ is $\Sigma_{\boldsymbol{b}}$. Given a multivariate uniformly distributed random vector $z \in [0, 1]^k$ consisting of k independent variables, there exists a generator function $\boldsymbol{b'} = \hat{r}(\boldsymbol{z})$, $\boldsymbol{b'} = \{b'_1, \cdots, b'_k\}$ such that $b'_i \sim \mathcal{F}_{b_i}, i \in [1, k]$, and $\Sigma_{\boldsymbol{b'}} \cong \Sigma_{\boldsymbol{b}}$.

Proof. The function $\hat{r}(\cdot)$ exists and can be constructed by first introducing an intermediate multivariate normal random vector $\boldsymbol{a} \sim \mathcal{N}(\boldsymbol{0}, \Sigma_{\boldsymbol{a}})$, and then applying the following transformations:

(a) NORTA [56], [57], which transforms vector $\boldsymbol{a}$ into vector $\boldsymbol{b'} = \{b'_1, \cdots, b'_k\}$ with $b'_i \sim \mathcal{F}_{b_i}, i \in [1, k]$ and the corresponding covariance matrix $\Sigma_{\boldsymbol{b'}} \cong \Sigma_{\boldsymbol{b}}$ by adjusting the covariance matrix $\Sigma_{\boldsymbol{a}}$ of $\boldsymbol{a}$.

$$b'_i = \mathcal{F}_{b_i}^{-1}\left[\Phi(a_i)\right], i \in [1, k], \tag{5}$$

where $\Phi(\cdot)$ denotes the univariate standard normal cdf and $\mathcal{F}_{b_i}^{-1}(\cdot)$ denotes the inverse of $\mathcal{F}_{b_i}$. To achieve $\Sigma_{\boldsymbol{b'}} \cong \Sigma_{\boldsymbol{b}}$, a matrix $\Lambda_{\boldsymbol{a}}$ that denotes the covariance of the input vector $\boldsymbol{a}$ can be uniquely determined [58]. If $\Lambda_{\boldsymbol{a}}$ is a feasible covariance matrix (symmetric and positive semi-definite with unit diagonal elements; a necessary but insufficient condition), $\Sigma_{\boldsymbol{a}}$ can be set to $\Lambda_{\boldsymbol{a}}$. Otherwise, $\Sigma_{\boldsymbol{a}}$ can be approximated by solving the following equation:

$$\begin{aligned} &\arg\min_{\Sigma_{\boldsymbol{a}}} \mathcal{D}(\Sigma_{\boldsymbol{a}}, \Lambda_{\boldsymbol{a}}) \\ &\text{subject to } \Sigma_{\boldsymbol{a}} \geq 0, \Sigma_{\boldsymbol{a}}(i, i) = 1 \end{aligned} \tag{6}$$

where $\mathcal{D}(\cdot)$ is a distance function [57].

13. https://github.com/dmlc/mxnet/

(b) Inverse transformation [59] to generate $\boldsymbol{a} \sim \mathcal{N}(\mathbf{0}, \Sigma_{\boldsymbol{a}})$ from multivariate uniformly distributed random vector $\boldsymbol{z} = \{z_1, \cdots, z_k\}$, where $z_i \sim \mathbf{U}(0,1), i \in [1,k]$.

$$\boldsymbol{a} = \mathbf{M} \cdot \left[\Phi^{-1}(z_1), \cdots, \Phi^{-1}(z_k)\right]' \tag{7}$$

where M is a lower-triangular, non-singular, factorization of $\Sigma_{\boldsymbol{a}}$ such that $\mathbf{M}\mathbf{M}' = \Sigma_{\boldsymbol{a}}$, Φ^{-1} is the inverse of the univariate standard normal cdf [59].

This completes the proof. □

ACKNOWLEDGMENTS

This study was partially supported by a Hong Kong RGC grant (HKBU 12201414) and the Madam Kwok Chung Bo Fun Graduate School Development Fund, HKBU. The authors would like to thank Dr. Xiangyuan Lan and Miss Huiqi Deng for their helpful suggestions.

REFERENCES

[1] A. Adler, "Sample images can be independently restored from face recognition templates," in *IEEE Canadian Conference on Electrical and Computer Engineering*, vol. 2, 2003, pp. 1163–1166.

[2] J. Galbally, C. McCool, J. Fierrez, S. Marcel, and J. Ortega-Garcia, "On the vulnerability of face verification systems to hill-climbing attacks," *Pattern Recognition*, vol. 43, no. 3, pp. 1027–1038, 2010.

[3] M. Gomez-Barrero, J. Galbally, J. Fierrez, and J. Ortega-Garcia, "Face verification put to test: A hill-climbing attack based on the uphill-simplex algorithm," in *IAPR/IEEE International Conference on Biometrics*, 2012, pp. 40–45.

[4] Y. C. Feng, M.-H. Lim, and P. C. Yuen, "Masquerade attack on transform-based binary-template protection based on perceptron learning," *Pattern Recognition*, vol. 47, no. 9, pp. 3019–3033, 2014.

[5] N. Erdogmus and S. Marcel, "Spoofing face recognition with 3d masks," *IEEE Transactions on Information Forensics and Security*, vol. 9, no. 7, pp. 1084–1097, July 2014.

[6] D. Wen, H. Han, and A. K. Jain, "Face spoof detection with image distortion analysis," *IEEE Transactions on Information Forensics and Security*, vol. 10, no. 4, pp. 746–761, 2015.

[7] K. Patel, H. Han, and A. K. Jain, "Secure face unlock: Spoof detection on smartphones," *IEEE Transactions on Information Forensics and Security*, 2016.

[8] S. Liu, P. C. Yuen, S. Zhang, and G. Zhao, "3d mask face anti-spoofing with remote photoplethysmography," in *European Conference on Computer Vision*. Springer, 2016, pp. 85–100.

[9] A. Mignon and F. Jurie, "Reconstructing faces from their signatures using rbf regression," in *British Machine Vision Conference*, 2013.

[10] P. Mohanty, S. Sarkar, and R. Kasturi, "From scores to face templates: a model-based approach," *IEEE Transactions on Pattern Analysis and Machine Intelligence*, vol. 29, no. 12, pp. 2065–2078, 2007.

[11] S. U. Hussain, T. Napoléon, and F. Jurie, "Face recognition using local quantized patterns," in *British Machive Vision Conference*, 2012.

[12] F. Schroff, D. Kalenichenko, and J. Philbin, "Facenet: A unified embedding for face recognition and clustering," in *IEEE Conference on Computer Vision and Pattern Recognition*, June 2015.

[13] B. Moghaddam, W. Wahid, and A. Pentland, "Beyond eigenfaces: Probabilistic matching for face recognition," in *IEEE International Conference on Automatic Face and Gesture Recognition*, 1998, pp. 30–35.

[14] M. A. Turk and A. P. Pentland, "Face recognition using eigenfaces," in *IEEE Conference on Computer Vision and Pattern Recognition*, June 1991, pp. 586–591.

[15] P. N. Belhumeur, J. P. Hespanha, and D. J. Kriegman, "Eigenfaces vs. fisherfaces: recognition using class specific linear projection," *IEEE Transactions on Pattern Analysis and Machine Intelligence*, vol. 19, no. 7, pp. 711–720, Jul 1997.

[16] P. C. Yuen and J.-H. Lai, "Face representation using independent component analysis," *Pattern Recognition*, vol. 35, no. 6, pp. 1247–1257, 2002.

[17] T. Ahonen, A. Hadid, and M. Pietikainen, "Face description with local binary patterns: Application to face recognition," *IEEE Transactions on Pattern Analysis and Machine Intelligence*, vol. 28, no. 12, pp. 2037–2041, 2006.

[18] O. Déniz, G. Bueno, J. Salido, and F. De la Torre, "Face recognition using histograms of oriented gradients," *Pattern Recognition Letters*, vol. 32, no. 12, pp. 1598–1603, 2011.

[19] D. Chen, X. Cao, F. Wen, and J. Sun, "Blessing of dimensionality: High-dimensional feature and its efficient compression for face verification," in *IEEE Conference on Computer Vision and Pattern Recognition*, June 2013, pp. 3025–3032.

[20] Y. Sun, Y. Chen, X. Wang, and X. Tang, "Deep learning face representation by joint identification-verification," in *Advances in Neural Information Processing Systems*, 2014, pp. 1988–1996.

[21] Y. Sun, X. Wang, and X. Tang, "Deeply learned face representations are sparse, selective, and robust," in *IEEE Conference on Computer Vision and Pattern Recognition*, 2015, pp. 2892–2900.

[22] O. M. Parkhi, A. Vedaldi, and A. Zisserman, "Deep face recognition," in *British Machine Vision Conference*, 2015.

[23] X. Wu, R. He, and Z. Sun, "A lightened cnn for deep face representation," *arXiv:1511.02683*, 2015.

[24] E. Learned-Miller, G. B. Huang, A. RoyChowdhury, H. Li, and G. Hua, "Labeled faces in the wild: A survey," in *Advances in Face Detection and Facial Image Analysis*. Springer, 2016, pp. 189–248.

[25] L. Wolf, T. Hassner, and I. Maoz, "Face recognition in unconstrained videos with matched background similarity," in *IEEE Conference on Computer Vision and Pattern Recognition*, 2011, pp. 529–534.

[26] B. F. Klare, B. Klein, E. Taborsky, A. Blanton, J. Cheney, K. Allen, P. Grother, A. Mah, and A. K. Jain, "Pushing the frontiers of unconstrained face detection and recognition: Iarpa janus benchmark a," in *IEEE Conference on Computer Vision and Pattern Recognition*, 2015, pp. 1931–1939.

[27] I. Goodfellow, Y. Bengio, and A. Courville, *Deep Learning*. MIT Press, 2016, http://www.deeplearningbook.org.

[28] J. Mairal, F. Bach, J. Ponce, and G. Sapiro, "Online dictionary learning for sparse coding," in *International Conference on Machine Learning*. ACM, 2009, pp. 689–696.

[29] C. Vondrick, A. Khosla, H. Pirsiavash, T. Malisiewicz, and A. Torralba, "Visualizing object detection features," *International Journal of Computer Vision*, vol. 119, no. 2, pp. 145–158, 2016.

[30] M. D. Zeiler, D. Krishnan, G. W. Taylor, and R. Fergus, "Deconvolutional networks," in *IEEE Conference on Computer Vision and Pattern Recognition*, 2010, pp. 2528–2535.

[31] M. D. Zeiler, G. W. Taylor, and R. Fergus, "Adaptive deconvolutional networks for mid and high level feature learning," in *IEEE International Conference on Computer Vision*, 2011, pp. 2018–2025.

[32] D. Wang, C. Otto, and A. K. Jain, "Face search at scale," *IEEE Transactions on Pattern Analysis and Machine Intelligence*, 2016.

[33] C. Otto, D. Wang, and A. K. Jain, "Clustering millions of faces by identity," *IEEE Transactions on Pattern Analysis and Machine Intelligence*, To appear, 2017.

[34] A. Radford, L. Metz, and S. Chintala, "Unsupervised representation learning with deep convolutional generative adversarial networks," *arXiv:1511.06434*, 2015.

[35] A. B. L. Larsen, S. K. Sønderby, and O. Winther, "Autoencoding beyond pixels using a learned similarity metric," *arXiv:1512.09300*, 2015.

[36] X. Yan, J. Yang, K. Sohn, and H. Lee, "Attribute2image: Conditional image generation from visual attributes," in *European Conference on Computer Vision*. Springer, 2016, pp. 776–791.

[37] B. Biggio, P. Russu, L. Didaci, and F. Roli, "Adversarial biometric recognition: A review on biometric system security from the adversarial machine-learning perspective," *IEEE Signal Processing Magazine*, vol. 32, no. 5, pp. 31–41, 2015.

[38] S. Ioffe and C. Szegedy, "Batch normalization: Accelerating deep network training by reducing internal covariate shift," *arXiv:1502.03167*, 2015.

[39] V. Nair and G. E. Hinton, "Rectified linear units improve restricted boltzmann machines," in *International Conference on Machine Learning*, 2010, pp. 807–814.

[40] B. Amos, B. Ludwiczuk, and M. Satyanarayanan, "Openface: A general-purpose face recognition library with mobile applications," CMU-CS-16-118, Tech. Rep., 2016.

[41] D. Yi, Z. Lei, S. Liao, and S. Z. Li, "Learning face representation from scratch," *arXiv:1411.7923*, 2014.

[42] R. Gross, I. Matthews, J. Cohn, T. Kanade, and S. Baker, "The cmu multi-pose, illumination, and expression (multi-pie) face database," *CMU Robotics Institute. TR-07-08, Tech. Rep*, 2007.
[43] Random: Probability, mathematical statistics, stochastic processes. [Online]. Available: http://www.math.uah.edu/stat/
[44] N. Dokuchaev, *Probability theory: A complete one semester course*. World Scientific, 2015.
[45] D. Kingma and J. Ba, "Adam: A method for stochastic optimization," *arXiv:1412.6980*, 2014.
[46] L. El Shafey, C. McCool, R. Wallace, and S. Marcel, "A scalable formulation of probabilistic linear discriminant analysis: Applied to face recognition," *IEEE Transactions on Pattern Analysis and Machine Intelligence*, vol. 35, no. 7, pp. 1788–1794, 2013.
[47] P. J. Phillips, P. J. Flynn, T. Scruggs, K. W. Bowyer, J. Chang, K. Hoffman, J. Marques, J. Min, and W. Worek, "Overview of the face recognition grand challenge," in *IEEE Conference on Computer Vision and Pattern Recognition*, vol. 1, 2005, pp. 947–954.
[48] G. B. Huang, M. Mattar, H. Lee, and E. Learned-Miller, "Learning to align from scratch," in *Advances in Neural Information Processing Systems*, 2012.
[49] S. Liao, Z. Lei, D. Yi, and S. Z. Li, "A benchmark study of large-scale unconstrained face recognition," in *IEEE International Joint Conference on Biometrics*, 2014, pp. 1–8.
[50] T. Chen, M. Li, Y. Li, M. Lin, N. Wang, M. Wang, T. Xiao, B. Xu, C. Zhang, and Z. Zhang, "Mxnet: A flexible and efficient machine learning library for heterogeneous distributed systems," *arXiv:1512.01274*, 2015.
[51] Y. C. Feng, P. C. Yuen, and A. K. Jain, "A hybrid approach for generating secure and discriminating face template," *IEEE Transactions on Information Forensics and Security*, vol. 5, no. 1, pp. 103–117, 2010.
[52] K. Nandakumar and A. K. Jain, "Biometric template protection: Bridging the performance gap between theory and practice," *IEEE Signal Processing Magazine*, vol. 32, no. 5, pp. 88–100, 2015.
[53] G. Mai, M.-H. Lim, and P. C. Yuen, "Fusing binary templates for multi-biometric cryptosystems," in *IEEE Conference on Biometrics Theory, Applications and Systems*, 2015, pp. 1–8.
[54] M.-H. Lim, S. Verma, G. Mai, and P. C. Yuen, "Learning discriminability-preserving histogram representation from unordered features for multibiometric feature-fused-template protection," *Pattern Recognition*, vol. 60, pp. 706–719, 2016.
[55] G. Mai, M.-H. Lim, and P. C. Yuen, "Binary feature fusion for discriminative and secure multi-biometric cryptosystems," *Image and Vision Computing*, 2016.
[56] M. C. Cario and B. L. Nelson, "Modeling and generating random vectors with arbitrary marginal distributions and correlation matrix," Department of Industrial Engineering and Management Sciences, Northwestern University, Tech. Rep., 1997.
[57] S. Ghosh and S. G. Henderson, "Behavior of the norta method for correlated random vector generation as the dimension increases," *ACM Transactions on Modeling and Computer Simulation*, vol. 13, no. 3, pp. 276–294, 2003.
[58] S. G. Henderson, B. A. Chiera, and R. M. Cooke, "Generating dependent quasi-random numbers," in *IEEE Winter Simulation Conference*, vol. 1, 2000, pp. 527–536.
[59] M. E. Johnson, *Multivariate statistical simulation: A guide to selecting and generating continuous multivariate distributions*. John Wiley & Sons, 2013.

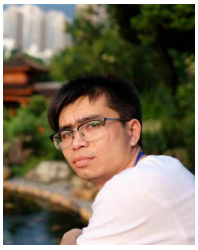

Guangcan Mai received the B.Eng degree in computer science and technology from South China University of Technology, Guangzhou, China, in 2013. He is currently pursuing the Ph.D degree in Computer Science from Hong Kong Baptist University, Hong Kong. He was a Visiting Scholar in the Pattern Recognition and Image Processing (PRIP) Lab, Michigan State University, USA. His research interests include biometric security, template protection, feature fusion and machine learning.

Pong C. Yuen received his B.Sc. degree in Electronic Engineering with First Class Honours in 1989 from City Polytechnic of Hong Kong, and his Ph.D. degree in Electrical and Electronic Engineering in 1993 from The University of Hong Kong. He joined the Hong Kong Baptist University in 1993 and, currently is a Professor and Head of the Department of Computer Science. Dr. Yuen was a recipient of the University Fellowship to visit The University of Sydney in 1996. In 1998, Dr. Yuen spent a 6-month sabbatical leave in The University of Maryland Institute for Advanced Computer Studies (UMIACS), University of Maryland at College Park. From June 2005 to January 2006, he was a visiting professor in GRAVIR laboratory (GRAphics, VIsion and Robotics) of INRIA Rhone Alpes, France. Dr. Yuen was the director of Croucher Advanced Study Institute (ASI) on biometric authentication in 2004 and the director of Croucher ASI on Biometric Security and Privacy in 2007. Dr. Yuen has been actively involved in many international conferences as an organizing committee and/or technical program committee member. He was the track co-chair of International Conference on Pattern Recognition (ICPR) 2006 and the program co-chair of IEEE Fifth International Conference on Biometrics: Theory, Applications and Systems (BTAS) 2012. Currently, Dr. Yuen is an Editorial Board Member of Pattern Recognition and Associate Editor of IEEE Transactions on Information Forensics and Security, and Senior Editor of SPIE Journal of Electronic Imaging. He is also serving as a Hong Kong Research Grant Council Engineering Panel Member. Dr. Yuen's current research interests include video surveillance, human face recognition, biometric security and privacy.

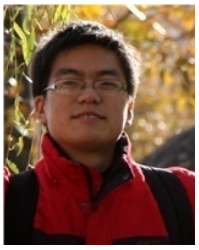

Kai Cao received the Ph.D. degree from Key Laboratory of Complex Systems and Intelligence Science, Institute of Automation, Chinese Academy of Sciences, Beijing, China, in 2010. He is currently a Post Doctoral Fellow in the Department of Computer Science and Engineering, Michigan State University, East Lansing. His research interests include biometric recognition, image processing and machine learning

Anil K. Jain is a University distinguished professor in the Department of Computer Science and Engineering at Michigan State University, East Lansing, Michigan. His research interests include pattern recognition and biometric authentication. He served as the editor-in-chief of the IEEE Transactions on Pattern Analysis and Machine Intelligence (1991-1994), a member of the United States Defense Science Board and The National Academies committees on Whither Biometrics and Improvised Explosive Devices. He has received Fulbright, Guggenheim, Alexander von Humboldt, and IAPR King Sun Fu awards. He is a member of the United States National Academy of Engineering and a Foreign Fellow of the Indian National Academy of Engineering.